Self-Assembly of Copper Sulfide Nanoparticles into Nanoribbons with Continuous Crystallinity

Guanxiang Ma,[†,‡] Yunlong Zhou,[‡] Xinyu Li,[‡,⊥] Kai Sun,[∥] Shaoqin Liu,[⊥] Junqing Hu,[†] and Nicholas A. Kotov[‡,§,⊥,∥,*]

[†]State Key Laboratory for Modification of Chemical Fibers and Polymer Materials, College of Materials Science and Engineering, Donghua University, China, [‡]Department of Chemical Engineering, University of Michigan, Ann Arbor, Michigan 48109, United States, [§]Biointerfaces Institute, University of Michigan, Ann Arbor, Michigan 48109, United States, [⊥]Key Laboratory of Microsystems and Microstructures Manufacturing, Harbin Institute of Technology, Harbin 150080, China, and [∥]Department of Materials Science and Engineering, University of Michigan, Ann Arbor, Michigan 48109, United States

ABSTRACT Copper chalcogenide nanoparticles (NPs) represent a promising material for solar energy conversion, electrical charge storage, and plasmonic devices. However, it is difficult to achieve high-quality NP dispersions in experimentally convenient and technologically preferred aqueous media. Also problematic is the transition from NP dispersion to continuously crystalline nanoscale materials, for instance, nanowires, nanoribbons, or similar high aspect ratio nano/microstructures capable of charge transport necessary for such applications. All previous examples of copper sulfide assemblies contained insulating gaps between NPs. Here we show that aqueous synthesis of high-quality monodispersed high-chalcocite β-Cu_2S NPs, with sizes from 2 to 10 nm, is possible. When reaction time increased, the NP shape evolved from nearly spherical particles into disks with predominantly hexagonal shape. Moreover, the monodispersed β-Cu_2S NPs were found to spontaneously self-assemble into nanochains and, subsequently, to nanoribbons. The width and length of the nanoribbons were 4–20 nm and 50–950 nm, respectively, depending on the assembly conditions. We observed the formation of the nanoribbons with continuous crystal lattice and charge transport pathways, making possible the utilization of self-assembly processes in the manufacturing of photovoltaic, plasmonic, and charge storage devices.

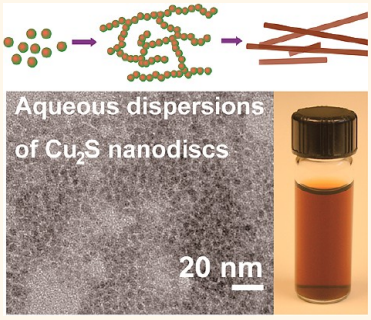

KEYWORDS: nanoparticles · copper sulfide · chalcocite · copper chalcogenide · aqueous dispersions · nanoribbons · self-organization · nanodisks · solar energy · charge storage · plasmonic particles

Despite the decades of research effort put into the syntheses of semiconductor nanoparticles (NPs), the need for novel methods of their preparation conducive to their use in solar cells, medical applications, and biosensors is still urgent. Such methods of synthesis need to combine simplicity and high quality of the dispersions. To be practical, these new synthetic methods must be driven by factors such as environmental friendliness and low cost while enabling solution processability of electronic devices. Among current NP syntheses, copper sulfide (Cu_2S, or chalcocite) is of particular interest, because of its affordability and low toxicity, while showing promising photovoltaic capabilities as a p-type semiconductor and plasmonic material.[1−3] It has a bulk band gap of 1.2 eV and has been investigated for use in solar cells,[4−7] field emission cold cathodes,[8,9] nanoscale switches,[10−12] and sensors.[13,14] In the past few years, various methods have been reported for the preparation of Cu_2S NPs *via* solution chemistry, such as high-temperature organic-phase solution methods,[7,15−18] water-in-oil interface confined methods,[19,20] ionic (cation and anion) exchange methods,[4,21−23] and hydrothermal methods.[24−26] For instance, S. Li *et al.*[17] synthesized monodispersed spherical Cu_2S NPs (sizes ranged from 2 to 20 nm) by the reaction of copper stearate and dodecanethiol in 1-octadecene. Z. Zhuang *et al.*[19] reported a method for the synthesis of monodispersed Cu_2S NPs in an autoclave at 200 °C at the water-in-oil interface. P. K. Jain *et al.*[21] used ion exchange in anhydrous toluene to convert CdSe/CdS nanorods (NRs) to Cu_2Se/Cu_2S NRs with reported diameters of 4 nm and lengths of 40 nm. C. Kuo *et al.*[22] used cubic and octahedral Cu_2O, with side lengths of 500 nm, as sacrificial templates for the growth of Cu_2S

* Address correspondence to kotov@umich.edu.

Received for review July 11, 2013 and accepted July 26, 2013.

Published online July 26, 2013
10.1021/nn4035525

© 2013 American Chemical Society

nanocages with wall thicknesses of 10−20 nm in ethanol using a controlled sulfidation and acid-etching process.

Syntheses of various Cu_2S nanostructures such as nanospheres (sizes from 3 to 50 nm),[27] nanodisks (14−20 nm in diameter and 5−7 nm thick),[28,29] NRs,[30,31] and nanowires (NWs) with diameters of 2−6 nm and lengths ranging from 100 to several thousands nm have also been reported.[32,33] A common thread among each of these syntheses is that the NPs have all been prepared in organic solutions and/or employed organometallic compounds. While yielding high-quality NPs, these methods are problematic, in that they involve undesirable high costs and highly toxic reagents. Furthermore, the presence of long-chain hydrophobic capping agents, such as ammonium diethyldithiocarbamate,[7] tetraoctylammonium bromide, trioctylamine,[28] dodecanethiol,[15,19] and octadecene,[17] creates a high barrier for electron tunneling between the NPs, restricting their use in solar cells and other applications and complicating solution processability of the electronic devices.[34−39] Synthesis in aqueous media is desirable because it eliminates some of the problematic issues just discussed; it is environmentally friendly, less toxic, and does not require long-chain, lipophilic capping agents.

Aqueous synthesis of II−VI semiconductor NPs, such as CdS,[40,41] CdSe,[42] CdTe,[43,44] ZnSe,[45] and HgTe,[46] by employing various short-chain stabilizing agents provides a useful alternative to common synthetic routes involving organic solvents with high boiling points. To date, however, these processes have yielded only poor-quality copper sulfide NPs. The aqueous dispersions typically consist of large particles (50−500 nm) with high polydispersity.[47] Furthermore, the reported copper sulfide particles are often formed from mixed crystalline phases and show low crystallinity.[48] In addition to broadening optical features, the interfaces between different phases create low-energy traps, which are detrimental for charge carrier mobility. The slowly occurring hydrolysis/oxidation of the poorly protected nanoscale colloids may also present a problem for devices that would not survive oxidation/hydrolysis conditions.[49,50] Therefore, the efficient synthesis of Cu_2S NPs with small and uniform size distribution in aqueous media remains a significant challenge and an opportunity for broad scientific advances.

An additional incentive to investigate the synthesis of Cu_2S in aqueous media is the possibility of creating technological processes based on self-assembly.[51] This process mimics the self-assembly of nanoscale biomolecules, such as proteins, DNAs, peptides, lipids, sugars, *etc*. Water is probably the most advantageous among all solvents to use in different self-organization processes because of the large variety of forces that manifest in water. Rather than contending with van der Waals forces, electrostatic repulsions, and steric interactions dominant in organic solvents, water allows other, intermolecular forces to make much greater contributions to self-assembly, resulting in more dynamic[52] and complex structures as seen in nature. Such forces include hydrogen bonding, hydrophobic interactions, dipole−dipole interactions,[53−55] excluded volume interactions, and correlated ionic attraction. Variation of ionic strength and pH affords an exceptionally wide range of control over many of these forces. Another factor that could be important for the assemblies is the variability of the interactions with respect to different NP facets, *i.e*., anisotropy of the interactions. Some contributions, exemplified by dipolar interactions, can even change signs and switch from positive to negative depending on the directions in 3D space.[54,55] Even the strength of seemingly long-range and isotropic electrostatic interactions can vary considerably, depending on the particle orientation especially for highly anisotropic colloids.[56,57] In water such directional variability is exacerbated due to a larger number of forces involved and greater differences in the structure of absorbed layers, ionic atmospheres, *etc*. Inorganic solvent pair potentials between NPs are often broadened, and anisotropy is reduced due to thicker stabilizer coatings.[58,59] While isotropic interactions of nearly spherical NPs could also lead to a very large variety of extended structures and superlattices the anisotropic interactions can produce complex terminal assemblies, wires, chains, and networks comparable in complexity to biological nanoassemblies.[60]

The chalcocite Cu_2S has three different phases that occur at different temperatures.[61] One is a monoclinic phase (low-chalcocite, α-Cu_2S) formed below 104 °C in bulk. It changes to a hexagonal phase (high-chalcocite, β-Cu_2S) at 104 °C in bulk and further transforms to a cubic phase (cubic-chalcocite, γ-Cu_2S) at 436 °C.[62] The hexagonal phase lattice is intrinsically anisotropic and has a unique (001) axis, which allows one to tailor the NP shape and engineer the packing symmetry of the NPs into superlattices. For instance, Z. Zhuang *et al*.[19] reported that anisotropic Cu_2S NPs with a dipole moment along the [001] direction self-assemble into a multilayer superlattice at the water-in-oil interface driven by hydrophobic interactions originating from the use of dodecanethiol as a capping agent. S. Li *et al*.[17] observed the assembly of Cu_2S NPs into two-dimensional (2D) and three-dimensional (3D) superlattices. Researchers in Li's laboratory,[63] as well as those in B. Korgel's group,[28,29] observed the self-assembly of Cu_2S hexagonal nanoplates into columns. These results show the possibility of constructing superstructures applicable to solar cell conversion and other applications by self-assembly of NPs. However, to be useful these methods require extraordinarily uniform NPs. Note that these assemblies took place in organic media and carried thick stabilizer shells that gave rise to the issues discussed above and impeded the potential

applications for which they were intended. To date, there has been no published account of an aqueous synthesis and assembly of Cu_2S NPs into nano/microscale structures with high aspect ratio and lattice-to-lattice connectivity between constitutive NPs. Previous examples of CdTe[64] and PbS[65] NPs synthesized in aqueous media indicated that the self-assembly with continuity in the semiconductor lattice is realistic. Recent observation[62] of the lowering of the phase transition temperature from monoclinic phase (low-chalcocite, α-Cu_2S) to hexagonal phase (high-chalcocite, β-Cu_2S), from 104 °C to 65 °C, yielded NRs with dimensions of 5 × 28 nm. These results indicated that recrystallization of NP assemblies in the production of monocrystalline nanoribbons or other nanoscale materials without gaps between original "building blocks" is also possible.

In this paper, we report a new, simple, and aqueous synthesis of β-Cu_2S NPs in a high-chalcocite hexagonal phase, producing dispersions of high size and shape uniformity. Both small, nearly spherical, and discoid NPs with predominantly hexagonal shapes ranging from 2 to 10 nm in size were obtained. Following the previous technique[64] of partial destabilization of NP dispersions, these β-Cu_2S NPs self-assembled into nanochains or nanoribbons with lattice-to-lattice connectivity between NPs 4−20 nm in width and 50−950 nm in lengths at low temperature (30 °C).

RESULTS AND DISCUSSION

Aqueous dispersions of thioglycolic acid (TGA)-stabilized nearly spherical NPs were obtained using the Rogach−Weller method previously developed for CdTe,[64] modified to use a 1:2:1 molar ratio of [Cu^+]/[TGA]/[TAA (thioacetamide)], and a reaction time of 1 h at 85 °C (Figure 1a and b). The process yielded NPs with a diameter of 3.3 ± 0.4 nm and a narrow size distribution (Figure 1b inset). The selected-area electron diffraction (SAED) pattern clearly shows the polycrystalline nature of the NPs (Figure 1c) with diffraction rings corresponding to (002), (101), (102), (110), (103), and (112) reflections, characteristic for the hexagonal phase of β-Cu_2S. For the crystal structure of hexagonal phase β-Cu_2S (Figure 1a inset), sulfur atoms occupy the hexagonal sulfur lattice frame, and Cu atoms insert into tetrahedral, trigonal, and linear voids.[61] The phase and purity of the prepared Cu_2S NPs were confirmed by the X-ray diffraction (XRD) pattern (Figure 1d). All of the diffraction peaks (upper curve) were indexed to the hexagonal β-Cu_2S standard (bottom curve: the XRD pattern from the standard β-Cu_2S powder on JCPDS card no. 26-1116, a = 3.961 nm, c = 6.722 nm); no peaks from other phases could be detected.

Energy-dispersive X-ray spectroscopy (EDS) was used to determine the Cu:S ratio as 2.0:1.32 (Figure S1), indicating that there was some excess of S in the

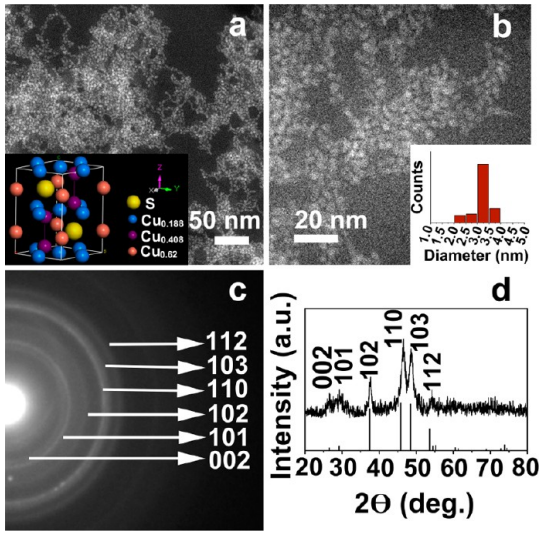

Figure 1. (a, b) Scanning transmission electron microscopy annular dark-field (STEM-ADF) images. (c) SAED pattern, and (d) XRD patterns of the β-Cu_2S NPs synthesized after 1 h reaction time. Inset in (a): schematic diagram of crystal structure. Inset in (b): size distribution. In (d) the curve represents XRD pattern of the NPs, while the bars represent the standard β-Cu_2S powder from JCPDS card no. 26-1116.

products compared to theoretical stoichiometry of β-Cu_2S. This excess likely originates from the TGA capping ligands that passivate the NP surface. The composition and valence states of β-Cu_2S NPs were studied by X-ray photoelectron spectroscopy (XPS) and Auger electron spectroscopy (AES) (Figure S2). To calibrate the spectra, the binding energy for C (1s) was used as an internal reference to eliminate the charging effect. A survey spectrum of the synthesized β-Cu_2S NPs identified the presence of Cu and S (Figure S2a).[66,67] High-resolution XPS spectra of Cu 2p and S 2p were collected to determine the oxidation states of the constituent elements. The binding energies of copper $2p_{3/2}$ and $2p_{1/2}$ for Cu_2S were 932.4 and 952.2 eV, respectively; the peak separation of 19.8 eV was indicative of Cu(I). No "shakeup" peaks were found in the higher binding energy direction, which was consistent with the standard reference XPS spectrum of Cu 2p in β-Cu_2S (Figure S2b).[68] Considering the proximity of the binding energies for Cu(0) and Cu(I), Cu LMM Auger spectroscopy was used to prove the valence state of Cu in the prepared samples (Figure S2d). The binding energy of Cu LMM was centered at 570.4 eV and was consistent with the literature values.[18] This result ruled out the possibility of Cu(0) in the samples, as the binding energy of monatomic Cu LMM is centered at 569.2 eV. The sulfur $2p_{3/2}$ and $2p_{1/2}$ peaks in the spectra (Figure S2c) were located at 162.0 and 163.2 eV, respectively, with a doublet separation of 1.2 eV. These positions match well with our expectation for S in sulfide phases based on previous studies.[22,24,63]

When the reaction time reached 30 min, small, spherical β-Cu_2S NPs formed with an average diameter

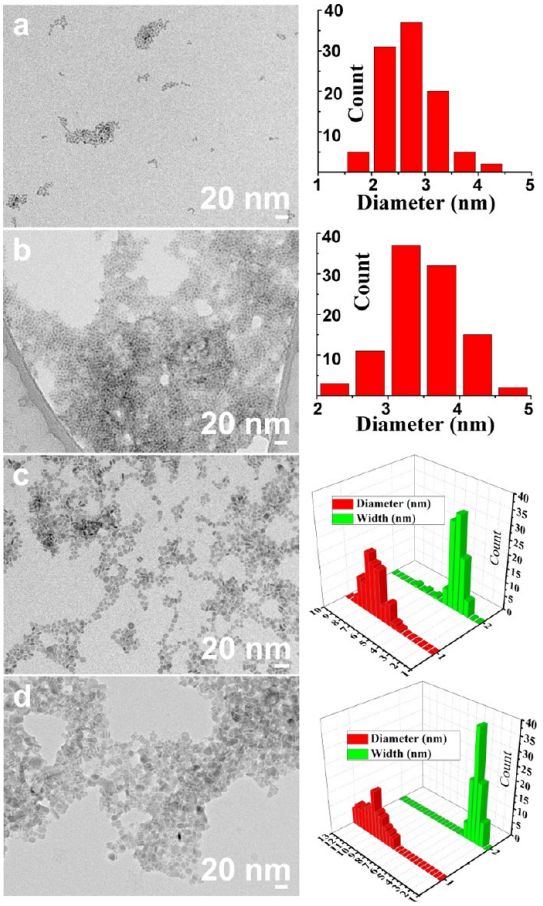

Figure 2. TEM bright-field images and size distributions of as-synthesized β-Cu_2S NPs with reaction times of (a) 30 min, (b) 1.5 h, (c) 2.5 h, and (d) 4 h.

of 2.6 ± 0.3 nm (Figure 2a). After 1.5 h of reaction at 85 °C, the NPs grew to a diameter of 3.8 ± 0.3 nm, still retaining high uniformity, narrow size distribution, and spherical shape (Figure 2b). The process exhibited a time-dependent evolution of both the size and shape of NPs. TEM images of the β-Cu_2S NPs revealed that small, nearly spherical particles (2.6 ± 0.3 nm) seen after 30 min reaction time transformed into nanodisks (10.2 ± 0.9 nm) at 4 h reaction time at 85 °C (Figures 2, Figure S3). At reaction t = 2 h, β-Cu_2S NPs transformed into nearly monodispersed nanodisks (Figure 3a). All synthesized particles and structures assembled from them revealed little in the UV−vis spectra in the 200−900 nm range (Figure S5). A high-magnification TEM image of the product demonstrated that the nanodisks tend to acquire hexagonal shapes approaching the geometry of hexagonal prisms. Since we still need to perfect the control of their geometry and to acquire the uniformity of their hexagonal form, as well as increase the resolution of electron microscopy images, we shall refer to them in this paper still as nanodisks. Note, however, that in relevant processes of self-organization (see Figures 4, 5) we do see the indications of their behavior as hexagonal prisms.

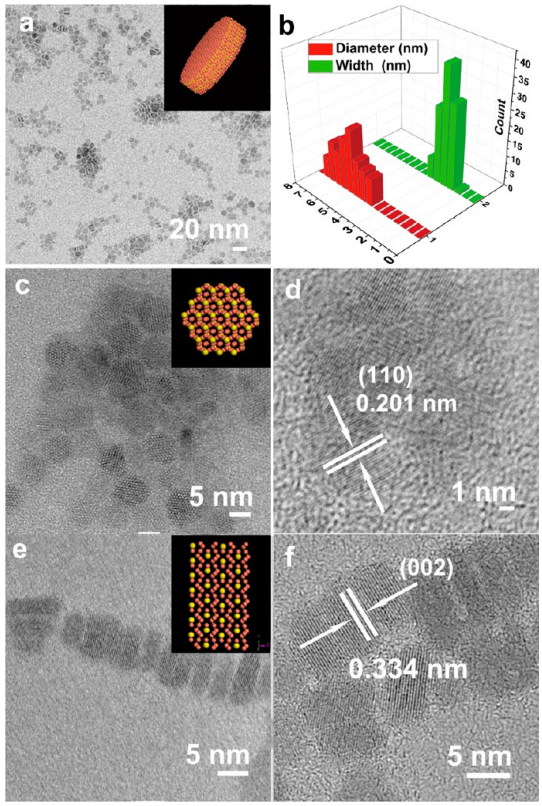

Figure 3. (a) TEM bright-field images, (b) size distributions, and (c, d, e, f) HRTEM images of the β-Cu_2S NPs synthesized after 2 h reaction time. Although the perfection of shapes was not achieved in this synthesis, many of them have a tendency to acquire a hexagonal shape. The insets in (a, c, e) show atomic models of the disks viewed from different directions; Cu atoms and V_{Cu} (vacancies of Cu atoms) are orange, and S atoms are yellow.

In 2D projection, typical for TEM, the nanodisks may appear to be rods and disks only because some NPs were facing down and some were standing perpendicularly aligned to the substrate. The diameter of the nanodisks was 5.5 ± 0.9 nm, while their height was 2.2 ± 0.4 nm (Figure 3b). The lattice fringes of face-down β-Cu_2S nanodisks showed a spacing of d = 0.201 nm (Figure 3c,d), which corresponds to the (110) lattice plane of the hexagonal phase of β-Cu_2S (the inset is an atom's view model along the [001] direction). The lattice fringes of a stand-up nanodisks (Figure 3e,f) showed a spacing of d = 0.334 nm (the inset is an atom's view model from the [110] orientation). This interatomic distance corresponds to the (002) lattice plane of the hexagonal phase of β-Cu_2S. When the reaction time was increased to 2.5 h, the particles grew to diameters of 6.7 ± 0.5 nm and widths of 2.6 ± 0.4 nm (Figure 2c). The nanodisks then grew to 10.2 ± 0.9 nm and 2.9 ± 0.3 nm in diameter and width, respectively, for 4 h reaction times. At this point the disks tended to stack together into chains (Figure 2d).

β-Cu_2S NPs were found to spontaneously assemble into high aspect ratio nano/microstructures after partial removal of the stabilizer in a previously reported

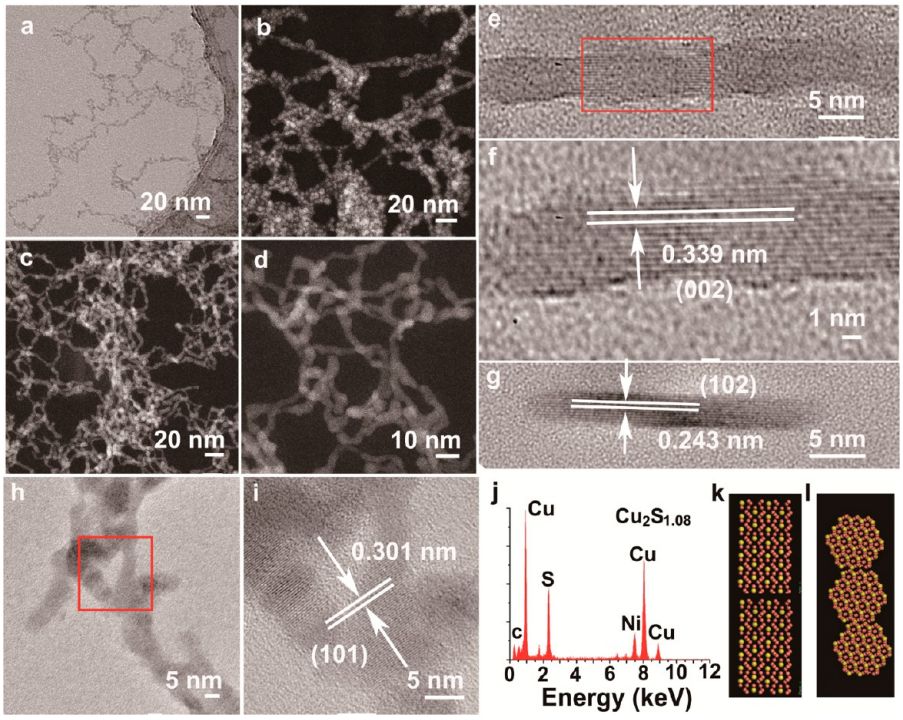

Figure 4. (a) TEM bright-field and (b) STEM-ADF images of the chains; (c, d) DF-STEM images of the nanoribbons; (e–i) HRTEM images of an individual nanoribbons; (j) EDS spectrum of the β-Cu_2S nanoribbons (the carbon and the nickel signals come from the nickel grid coated by carbon film) of as-synthesized β-Cu_2S NPs after partial stabilizer removal for different times; (k, l) atomic models of the nanoribbons viewed from different directions; Cu atoms and V_{Cu} (vacancies of Cu atoms) are orange, and S atoms are yellow.

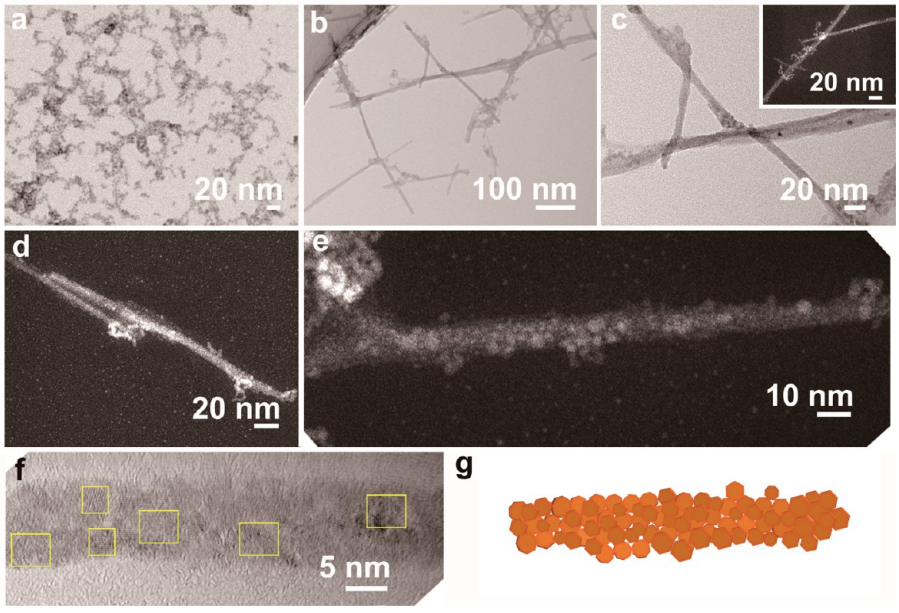

Figure 5. (a) TEM bright-field images of nanodisks assembled into chains; (b, c) TEM bright-field images of nanoribbons assembled from β-Cu_2S nanodisks; (d, e) STEM-ADF images of the nanoribbons with clearly visible individual nanodisks; (f) HRTEM images of an individual nanoribbon; areas of crystallinity corresponding to individual β-Cu_2S nanodisks are indicated with yellow lines; (g) schematic diagram of the nanoribbon assembled from β-Cu_2S nanodisks represented by the hexagons.

precipitation–redispersion process.[64] As-synthesized spherical β-Cu_2S NPs with a diameter of 3.3 $\pm$ 0.4 nm assembled into nanochains (24 h), and then the chains assembled into a network (Figure 4a,b). When we prolonged the assembly time to one week, the chains fused gradually into nanoribbons with lattice-to-lattice connectivity including the formation of epitaxial single-crystalline wires (Figure 4e–i). To understand better the crystallography of the nanoribbons, we measured lattice fringe spacing in them. Three different lattice fringe spacings were found in nanoribbons: 0.339 nm (Figure 4e,f), 0.243 nm (Figure 4g), and 0.301 nm

(Figure 4h,i), which corresponded to the (002), (102), and (101) lattice planes of hexagonal β-Cu_2S, respectively. Therefore, nanoribbons form with the *c*-axis of β-Cu_2S oriented both along, with, and perpendicular to the long axis of the nanoribbons, which would be quite characteristic of flat hexagonal prisms tiling the surface. The width of the nanoribbons ranged from 3 to 5 nm (Figure 4d), and their length ranged from 42 to 97 nm (Figure S4b). EDS spectroscopy indicated that the Cu:S ratio was 2.0:1.08 (Figure S1). Note that the ratio of S significantly decreased in the assembled nanoribbons compared to the ratio for the original NPs, which should be expected due to removal of the TGA stabilizer. The fact that NP self-assembly resulted in nanoribbons forming a continuous crystal lattice clearly indicates the possibility of incorporating self-organization into technological processes for the manufacturing of electronic devices. The direct transition from NPs to continuous nanoribbons has not been realized in any reported processes taking place in organic media, with thick stabilizing coats made from insulating aliphatic surfactants.

We also investigated the assembly behavior of the β-Cu_2S nanodisks with a diameter of 5.5 $\pm$ 0.9 nm (Figure 5). The difference compared with the smaller nearly spherical Cu_2S NPs was that the nanodisks needed a longer time to assemble. Most NPs assembled into nanochains if the assembly continued for one week (Figure 5a). When we prolonged the assembly time to three weeks, polycrystalline nanoribbons with diameters of *ca.* 10 nm formed (Figure 5b–g), and the length of the wires ranged from 223 to 953 nm (Figure S4a).

As discussed in our previous article,[64] partial removal of the TGA stabilizer reduces the repulsive forces between the NPs, and thus the attractive dipole forces cause the NPs to form linear aggregates. If the 2-propanol–water precipitation–redispersion steps are excluded and the original excess thiol stabilizer was allowed to remain in solution, neither nanochains nor nanoribbons could form. After some time, the Cu_2S NPs with a small size (3.3 $\pm$ 0.4 nm) finally assembled into single-crystal nanoribbons. Ostwald ripening could drive the recrystallization process, but we also think there could be other mechanisms that could take place only in the confinement of the narrow gaps between NPs. For hexagonal phase β-Cu_2S (inset of Figure 1a), sulfur atoms occupy the hexagonal sulfur lattice frame, and Cu atoms insert into tetrahedral, trigonal, and linear voids.[61] The ions then diffuse to the NP chains, attaching to the inside of the agglomerates, filling in the voids between the NPs. The presence of a hexagonal motif in the shapes of the NPs with larger sizes of 5.5 $\pm$ 0.9 nm visible in Figure 3c is the likely the cause for the nanochains configuring into nanoribbons with lattice-to-lattice connectivity. Note here the relevance of the previous studies on oriented attachment, investigated predominantly for oxide systems that tend to occur with faceted NPs in polar solvents.[69–71] While monocrystallinity of nanoribbons (as in Figure 4) obtained in the process of oriented attachment with epitaxial match at the interfaces would be preferred for a variety of applications due to substantially faster charge transport,[72] the polycrystalline systems may actually be preferred for flexible devices because of their desirable mechanical properties and reduced dependence of electrical properties on strain.

CONCLUSIONS

In summary, a simple aqueous synthetic approach for size- and shape-controllable growth of NPs from the hexagonal high-chalcocite form of β-Cu_2S was reported. They tend to crystallize in the shape of nanodisks and imperfect hexagonal pyramids when reaching a size of *ca.* 5 nm. By partial removal of the stabilizer directly in aqueous solvents at low temperature, nanochains and nanoribbons were assembled from both small and large β-Cu_2S nanodisks. The formation of high aspect ratio nanoribbons is consistent with hexagonal tiling of the surfaces with NPs and leads to nano/microstructures with lattice-to-lattice connectivity. Evidence of self-assembly into monocrystalline form presumably *via* epitaxial match of particle surfaces was also found. One should expect a substantial increase of charge carrier mobility across the assembled structures compared to all the previous cases of assembled Cu_2S and other NP superstructures separated by insulating surfactants. The described assembly process should simplify the preparation of solution-processed electronic devices from NPs reported before.[34–39] Potentially, improvement of hole mobility[8,73] might be expected compared to other solution processes for copper sulfide devices[7] and organic electronic materials[13,25] but should be investigated experimentally in detail.

The constituent elements of these structures are nontoxic and abundant, allowing for a wide range of applications. Moreover, they could be used as templates for the preparation of multielement metal chalcogenides in aqueous solution, such as $CuInS_2$, Cu_2ZnSnS_4, and $CuInGaSe_2$, which are long-standing candidates for solar energy conversion. Their assembly into 2D structures could strengthen their potential for use as practical solar absorber layers, where directional orientation and length control will likely allow for enhanced efficiencies.

METHODS

Chemicals. Copper(I) chloride (CuCl, $\geq$99.99%), thioglycolic acid solution ($C_2H_4O_2S$, TGA, 70% (w/w) in H_2O), thioacetamide (C_2H_5NS, $\geq$99.0%), sodium hydroxide (NaOH, $\geq$98%), and 2-propanol (99.5%) were all purchased from Aldrich. E-pure deionized water (18.2 M$\Omega\cdot$cm) was obtained from a Millipore Milli-Q system. All of

the chemicals were used as received without any further purification.

Synthesis of β-Cu_2S NPs. In a typical synthesis, 100 mL of deionized water was heated to 85 °C in a three-neck flask (150 mL) fitted with a valve and deaerated by bubbling 99.99% nitrogen under magnetic stirring for 30 min to remove residual oxygen. Thioglycolic acid (2 mmol, 0.14 mL) was injected while stirring and continuously purging the reaction media with nitrogen for 30 min. Copper(I) chloride (1 mmol, 0.099 g) powder was quickly added to the flask by opening a bottle stopper while keeping positive nitrogen pressure, then closing the bottle stopper. The entire process was done within several seconds to prevent air entry into the flask. After refluxing for 1 h at 85 °C, a white, thick emulsion formed. The pH of the media was adjusted to 9.0 by adding a 0.5 M solution of sodium hydroxide. The solution became clear and transparent after about 1 min. After 5 min, a solution of thioacetamide (TAA), obtained by dissolution of 0.0375 g (0.5 mmol) of TAA in 2 mL of deionized water, was injected into the reaction media all at once. The color of the solution turned light brown after 0.5 h, indicating the formation of the β-Cu_2S nanocolloids; the color continued to deepen, gradually changing to a dark brown after 4 h. As explained, the time of reflux determined the diameter of the resulting NPs. Then the solution was cooled to room temperature by purging with nitrogen gas.

Self-Assembly of β-Cu_2S NPs. A 10 mL amount of the resulting NPs taken from the reaction media was added into the centrifuge tube; then 20 mL of 2-propanol was slowly added to the same tube. The tube was shaken until the mixture became homogeneous (5 min). A dark brown and black powder was obtained after centrifugation at 8000 rpm for 10 min. The final precipitate was redispersed in pH 9.0 DI water (50 mL) at room temperature. The dispersion was incubated for three weeks in an evacuated container at 30 °C. All glassware was cleaned by immersing in *aqua regia* (HCl/HNO_3, 3:1) for 30 min, then kept in an ultrasonic washer at 60 °C for no less than 30 min, washed several times with alkali detergent, and finally rinsed with DI water. All glassware was then thoroughly dried in the oven at 80 °C before each use.

Conflict of Interest: The authors declare no competing financial interest.

Supporting Information Available: Material characterizations, energy-dispersive X-ray spectroscopy results, XPS survey spectra results, and size distributions of NPs are included. This material is available free of charge *via* the Internet at http://pubs.acs.org.

Acknowledgment. We acknowledge the financial assistance by the China Scholarship Council, the Innovation Foundation of DHU for PhD Graduates (No. 12D10619), and the PhD Programs Foundation of Ministry of Education of China (Grant No. 20110075110008). This material is also partially supported by the Center for Solar and Thermal Energy Conversion, an Energy Frontier Research Center funded by the U.S. Department of Energy, Office of Science, and Office of Basic Energy Sciences, under Award No. DE-SC0000957. We also greatly acknowledge the partial support from NSF under Grants ECS-0601345, EFRI-BSBA 0938019, CBET 0933384, CBET 0932823, and CBET 1036672. The authors thank the University of Michigan's EMAL for its assistance with electron microscopy.

REFERENCES AND NOTES

1. Luther, J. M.; Jain, P. K.; Ewers, T.; Alivisatos, A. P. Localized Surface Plasmon Resonances Arising from Free Carriers in Doped Quantum Dots. *Nat. Mater.* **2011**, *10*, 361–366.
2. Zhao, Y. X.; Pan, H. C.; Lou, Y. B.; Qiu, X. F.; Zhu, J. J.; Burda, C. Plasmonic $Cu_{2-x}S$ Nanocrystals: Optical and Structural Properties of Copper-Deficient Copper(I) Sulfides. *J. Am. Chem. Soc.* **2009**, *131*, 4253–4261.
3. Hsu, S. W.; Bryks, W.; Tao, A. R. Effects of Carrier Density and Shape on the Localized Surface Plasmon Resonances of $Cu_{2-x}S$ Nanodisks. *Chem. Mater.* **2012**, *24*, 3765–3771.
4. Tang, J.; Huo, Z.; Brittman, S.; Gao, H.; Yang, P. Solution-Processed Core-Shell Nanowires for Efficient Photovoltaic Cells. *Nat. Nanotechnol.* **2011**, *6*, 568–572.
5. Pan, C.; Niu, S.; Ding, Y.; Dong, L.; Yu, R.; Liu, Y.; Zhu, G.; Wang, Z. L. Enhanced Cu_2S/CdS Coaxial Nanowire Solar Cells by Piezo-Phototronic Effect. *Nano Lett.* **2012**, *12*, 3302–3307.
6. Xu, Q.; Huang, B.; Zhao, Y.; Yan, Y.; Noufi, R.; Wei, S. H. Crystal and Electronic Structures of Cu_xS Solar Cell Absorbers. *Appl. Phys. Lett.* **2012**, *100*, 061906.
7. Wu, Y.; Wadia, C.; Ma, W. L.; Sadtler, B.; Alivisatos, A. P. Synthesis and Photovoltaic Application of Copper(I) Sulfide Nanocrystals. *Nano Lett.* **2008**, *8*, 2551–2555.
8. Chen, J.; Deng, S. Z.; Xu, N. S.; Wang, S.; Wen, X.; Yang, S.; Yang, C.; Wang, J.; Ge, W. Field Emission from Crystalline Copper Sulphide Nanowire Arrays. *Appl. Phys. Lett.* **2002**, *80*, 3620–3622.
9. Wu, Q. B.; Ren, S.; Deng, S. Z.; Chen, J.; Xu, N. S. Growth of Aligned Cu_2S Nanowire Arrays with AAO Template and Their Field-Emission Properties. *J. Vac. Sci. Technol. B* **2004**, *22*, 1282–1285.
10. Sakamoto, T.; Sunamura, H.; Kawaura, H.; Hasegawa, T.; Nakayama, T.; Aono, M. Nanometer-Scale Switches Using Copper Sulfide. *Appl. Phys. Lett.* **2003**, *82*, 3032–3034.
11. Sakamoto, T.; Iguchi, N.; Aono, M. Nonvolatile Triode Switch Using Electrochemical Reaction in Copper Sulfide. *Appl. Phys. Lett.* **2010**, *96*, 252104.
12. Nayak, A.; Tsuruoka, T.; Terabe, K.; Hasegawa, T.; Aono, M. Switching Kinetics of a Cu_2S-Based Gap-Type Atomic Switch. *Nanotechnology* **2011**, *22*, 235201.
13. Lee, H.; Yoon, S. W.; Kim, E. J.; Park, J. In-Situ Growth of Copper Sulfide Nanocrystals on Multiwalled Carbon Nanotubes and Their Application as Novel Solar Cell and Amperometric Glucose Sensor Materials. *Nano Lett.* **2007**, *7*, 778–784.
14. Sagade, A. A.; Sharma, R.; Sulaniya, I. Enhancement in Sensitivity of Copper Sulfide Thin Film Ammonia Gas Sensor: Effect of Swift Heavy Ion Irradiation. *J. Appl. Phys.* **2009**, *105*, 043701.
15. Du, X. S.; Mo, M. S.; Zheng, R. K.; Lim, S. H.; Meng, Y. Z.; Mai, Y. W. Shape-Controlled Synthesis and Assembly of Copper Sulfide Nanoparticles. *Cryst. Growth Des.* **2008**, *8*, 2032–2035.
16. Tang, A.; Qu, S.; Li, K.; Hou, Y.; Teng, F.; Cao, J.; Wang, Y.; Wang, Z. One-Pot Synthesis and Self-Assembly of Colloidal Copper(I) Sulfide Nanocrystals. *Nanotechnology* **2010**, *21*, 285602.
17. Li, S.; Wang, H.; Xu, W.; Si, H.; Tao, X.; Lou, S.; Du, Z.; Li, L. S. Synthesis and Assembly of Monodisperse Spherical Cu_2S Nanocrystals. *J. Colloid Interface Sci.* **2009**, *330*, 483–487.
18. Mott, D.; Yin, J.; Engelhard, M.; Loukrakpam, R.; Chang, P.; Miller, G.; Bae, I. T.; Chandra Das, N.; Wang, C.; Luo, J.; *et al.* From Ultrafine Thiolate-Capped Copper Nanoclusters toward Copper Sulfide Nanodiscs: A Thermally Activated Evolution Route. *Chem. Mater.* **2010**, *22*, 261–271.
19. Zhuang, Z. B.; Peng, Q.; Zhang, B.; Li, Y. D. Controllable Synthesis of Cu_2S Nanocrystals and Their Assembly into a Superlattice. *J. Am. Chem. Soc.* **2008**, *130*, 10482–10483.
20. Tian, C.; Kang, Z.; Wang, E.; Gao, L.; Wang, C.; Xu, L.; Hu, C. Synthesis of Dodecanethiolate-Protected Cu_2S Nanoparticles in a Two-Phase System. *Mater. Lett.* **2005**, *59*, 1156–1160.
21. Jain, P. K.; Amirav, L.; Aloni, S.; Alivisatos, A. P. Nanoheterostructure Cation Exchange: Anionic Framework Conservation. *J. Am. Chem. Soc.* **2010**, *132*, 9997–9999.
22. Kuo, C. H.; Chu, Y. T.; Song, Y. F.; Huang, M. H. Cu_2O Nanocrystal-Templated Growth of Cu_2S Nanocages with Encapsulated Au Nanoparticles and In-Situ Transmission X-ray Microscopy Study. *Adv. Funct. Mater.* **2011**, *21*, 792–797.
23. Thimsen, E.; Peng, Q.; Martinson, A. B. F.; Pellin, M. J.; Elam, J. W. Ion Exchange in Ultrathin Films of Cu_2S and ZnS under Atomic Layer Deposition Conditions. *Chem. Mater.* **2011**, *23*, 4411–4413.
24. Lu, Q. Y.; Gao, F.; Zhao, D. Y. One-Step Synthesis and Assembly of Copper Sulfide Nanoparticles to Nanowires, Nanotubes, and Nanovesicles by a Simple Organic Amine-Assisted Hydrothermal Process. *Nano Lett.* **2002**, *2*, 725–728.

25. Chen, L.; Zou, Y.; Qiu, W.; Chen, F.; Xu, M.; Shi, M.; Chen, H. Hydrothermal Synthesis of Cu_2S Nanocrystalline Thin Film on Indium Tin Oxide Substrate: Morphology, Optical and Electrical Properties. *Thin Solid Films* **2012**, *520*, 5249–5253.
26. Yu, X.; An, X. Controllable Hydrothermal Synthesis of Cu_2S Nanowires on the Copper Substrate. *Mater. Lett.* **2010**, *64*, 252–254.
27. Ghezelbash, A.; Korgel, B. A. Nickel Sulfide and Copper Sulfide Nanocrystal Synthesis and Polymorphism. *Langmuir* **2005**, *21*, 9451–9456.
28. Sigman, M. B.; Ghezelbash, A.; Hanrath, T.; Saunders, A. E.; Lee, F.; Korgel, B. A. Solventless Synthesis of Monodisperse Cu_2S Nanorods, Nanodisks, and Nanoplatelets. *J. Am. Chem. Soc.* **2003**, *125*, 16050–16057.
29. Saunders, A. E.; Ghezelbash, A.; Smilgies, D. M.; Sigman, M. B.; Korgel, B. A. Columnar Self-assembly of Colloidal Nanodisks. *Nano Lett.* **2006**, *6*, 2959–2963.
30. Larsen, T. H.; Sigman, M.; Ghezelbash, A.; Doty, R. C.; Korgel, B. A. Solventless Synthesis of Copper Sulfide Nanorods by Thermolysis of a Single Source Thiolate-Derived Precursor. *J. Am. Chem. Soc.* **2003**, *125*, 5638–5639.
31. Kruszynska, M.; Borchert, H.; Bachmatiuk, A.; Rummeli, M. H.; Buchner, B.; Parisi, J.; Kolny-Olesiak, J. Size and Shape Control of Colloidal Copper(I) Sulfide Nanorods. *ACS Nano* **2012**, *6*, 5889–5896.
32. Chen, L.; Chen, Y. B.; Wu, L. M. Synthesis of Uniform Cu_2S Nanowires from Copper-Thiolate Polymer Precursors by a Solventless Thermolytic Method. *J. Am. Chem. Soc.* **2004**, *126*, 16334–16335.
33. Liu, Z. P.; Xu, D.; Liang, J. B.; Shen, J. M.; Zhang, S. Y.; Qian, Y. T. Growth of Cu_2S Ultrathin Nanowires in a Binary Surfactant Solvent. *J. Phys. Chem. B* **2005**, *109*, 10699–10704.
34. Lee, J. S.; Kovalenko, M. V.; Huang, J.; Chung, D. S.; Talapin, D. V. Band-Like Transport, High Electron Mobility and High Photoconductivity in All-Inorganic Nanocrystal Arrays. *Nat. Nanotechnol.* **2011**, *6*, 348–352.
35. Kim, D. K.; Lai, Y. M.; Diroll, B. T.; Murray, C. B.; Kagan, C. R. Flexible and Low-Voltage Integrated Circuits Constructed from High-Performance Nanocrystal Transistors. *Nat. Commun.* **2012**, *3*, 1–6.
36. Kovalenko, M. V.; Scheele, M.; Talapin, D. V. Colloidal Nanocrystals with Molecular Metal Chalcogenide Surface Ligands. *Science* **2009**, *324*, 1417–1420.
37. McDonald, S. A.; Konstantatos, G.; Zhang, S. G.; Cyr, P. W.; Klem, E. J. D.; Levina, L.; Sargent, E. H. Solution-Processed PbS Quantum Dot Infrared Photodetectors and Photovoltaics. *Nat. Mater.* **2005**, *4*, 138–142.
38. Tang, J.; Kemp, K. W.; Hoogland, S.; Jeong, K. S.; Liu, H.; Levina, L.; Furukawa, M.; Wang, X. H.; Debnath, R.; Cha, D. K.; Chou, K. W.; Fischer, A.; Amassian, A.; Asbury, J. B.; Sargent, E. H. Colloidal-Quantum-Dot Photovoltaics Using Atomic-Ligand Passivation. *Nat. Mater.* **2011**, *10*, 765–771.
39. Talapin, D. V.; Murray, C. B. PbSe Nanocrystal Solids for *n*- and *p*-Channel Thin Film Field-Effect Transistors. *Science* **2005**, *310*, 86–89.
40. Vossmeyer, T.; Katsikas, L.; Giersig, M.; Popovic, I. G.; Diesner, K.; Chemseddine, A.; Eychmuller, A.; Weller, H. CdS Nanoclusters-Synthesis, Characterization, Size-Dependent Oscillator Strength, Temperature Shift of the Excitonic-Transition Energy, and Reversible Absorbency Shift. *J. Phys. Chem.* **1994**, *98*, 7665–7673.
41. Govan, J. E.; Jan, E.; Querejeta, A.; Kotov, N. A.; Gun'ko, Y. K. Chiral Luminescent CdS Nano-Tetrapods. *Chem. Commun.* **2010**, *46*, 6072–6074.
42. Wuister, S. F.; Donega, C. D.; Meijerink, A. Influence of Thiol Capping on the Exciton Luminescence and Decay Kinetics of CdTe and CdSe Quantum. *J. Phys. Chem. B* **2004**, *108*, 17393–17397.
43. Wuister, S. F.; Donega, C. D. M.; Meijerink, A. Luminescence Temperature Antiquenching of Water-Soluble CdTe Quantum Dots: Role of the Solvent. *J. Am. Chem. Soc.* **2004**, *126* (33), 10397−10402.
44. Gaponik, N.; Talapin, D. V.; Rogach, A. L.; Hoppe, K.; Shevchenko, E. V.; Kornowski, A.; Eychmuller, A.; Weller, H. Thiol-Capping of CdTe Nanocrystals: An Alternative to Organometallic Synthetic Routes. *J. Phys. Chem. B* **2002**, *106*, 7177–7185.
45. Shavel, A.; Gaponik, N.; Eychmuller, A. Efficient UV-Blue Photoluminescing Thiol-Stabilized Water-Soluble Alloyed ZnSe(S) Nanocrystals. *J. Phys. Chem. B* **2004**, *108*, 5905–5908.
46. Rogach, A.; Kershaw, S.; Burt, M.; Harrison, M.; Kornowski, A.; Eychmuller, A.; Weller, H. Colloidally Prepared HgTe Nanocrystals with Strong Room-Temperature Infrared Luminescence. *Adv. Mater.* **1999**, *11*, 552–555.
47. Cao, H. L.; Qian, X. F.; Wang, C.; Ma, X. D.; Yin, J.; Zhu, Z. K. High Symmetric 18-Facet Polyhedron Nanocrystals of Cu_7S_4 with a Hollow Nanocage. *J. Am. Chem. Soc.* **2005**, *127*, 16024–16025.
48. Liufu, S. C.; Chen, L. D.; Yao, Q.; Huang, F. Q. In Situ Assembly of Cu_xS Quantum-Dots into Thin Film: A Highly Conductive *p*-Type Transparent Film. *J. Phys. Chem. C* **2008**, *112*, 12085–12088.
49. Partain, L. D.; Mcleod, P. S.; Duisman, J. A.; Peterson, T. M.; Sawyer, D. E.; Dean, C. S. Degradation of a Cu_xS/CdS Solar-Cell in Hot, Moist Air and Recovery in Hydrogen and Air. *J. Appl. Phys.* **1983**, *54*, 6708–6720.
50. Partain, L. D. A New Space-Charge-Limited-Current Diode Theory with Analysis of Cu_xS/CdS Data. *J. Appl. Phys.* **1983**, *54*, 5218–5226.
51. Xu, L.; Ma, W.; Wang, L.; Xu, C.; Kuang, H.; Kotov, N. A. Nanoparticle Assemblies: Dimensional Transformation of Nanomaterials and Scalability. *Chem. Soc. Rev.* **2013**, *42*, 3114–26.
52. Wang, L. B.; Xu, L. G.; Kuang, H.; Xu, C. L.; Kotov, N. A. Dynamic Nanoparticle Assemblies. *Acc. Chem. Res.* **2012**, *45*, 1916–1926.
53. Tang, Z. Y.; Zhang, Z. L.; Wang, Y.; Glotzer, S. C.; Kotov, N. A. Self-Assembly of CdTe Nanocrystals into Free-Floating Sheets. *Science* **2006**, *314*, 274–278.
54. Yang, M.; Sun, K.; Kotov, N. A. Formation and Assembly-Disassembly Processes of ZnO Hexagonal Pyramids Driven by Dipolar and Excluded Volume Interactions. *J. Am. Chem. Soc.* **2010**, *132*, 1860–1872.
55. Shanbhag, S.; Kotov, N. A. On the Origin of a Permanent Dipole Moment in Nanocrystals with a Cubic Crystal Lattice: Effects of Truncation, Stabilizers, and Medium for CdS Tetrahedral Homologues. *J. Phys. Chem. B* **2006**, *110*, 12211–12217.
56. Mourchid, A.; Delville, A.; Lambard, J.; Lecolier, E.; Levitz, P. Phase-Diagram of Colloidal Dispersions of Anisotropic Charged-Particles - Equilibrium Properties, Structure, and Rheology of Laponite Suspensions. *Langmuir* **1995**, *11*, 1942–1950.
57. Jiang, T. Y.; Zukoski, C. F. Rheology of Dense Suspensions of Shape Anisotropic Particles Designed to Show pH-Sensitive Anisotropic Pair Potentials. *J. Phys.: Condens. Matter* **2012**, *24*, 375109.
58. Xia, Y. S.; Nguyen, T. D.; Yang, M.; Lee, B.; Santos, A.; Podsiadlo, P.; Tang, Z. Y.; Glotzer, S. C.; Kotov, N. A. Self-Assembly of Self-Limiting Monodisperse Supraparticles from Polydisperse Nanoparticles. *Nat. Nanotechnol.* **2011**, *6*, 580–587.
59. Lilly, G. D.; Lee, J.; Sun, K.; Tang, Z.; Kim, K. S.; Kotov, N. A. Media Effect on CdTe Nanowire Growth: Mechanism of Self-Assembly, Ostwald Ripening, and Control of NW Geometry. *J. Phys. Chem. C* **2008**, *112*, 370–377.
60. Kotov, N. A. Inorganic Nanoparticles as Protein Mimics. *Science* **2010**, *330* (6001), 188−189.
61. Buerger, M. J.; Wuensch, B. J. Distribution of Atoms in High Chalcocite, Cu_2S. *Science* **1963**, *141*, 276–277.
62. Zheng, H. M.; Rivest, J. B.; Miller, T. A.; Sadtler, B.; Lindenberg, A.; Toney, M. F.; Wang, L. W.; Kisielowski, C.; Alivisatos, A. P. Observation of Transient Structural-Transformation Dynamics in a Cu_2S Nanorod. *Science* **2011**, *333*, 206–209.
63. Li, X. M.; Shen, H. B.; Niu, J. Z.; Zhang, Y. G.; Wang, H. Z.; Li, L. S. Columnar Self-Assembly of Cu_2S Hexagonal

Nanoplates Induced by Tin(IV)-X Complex as Inorganic Surface Ligand. *J. Am. Chem. Soc.* **2010**, *132*, 12778–12779.
64. Tang, Z. Y.; Kotov, N. A.; Giersig, M. Spontaneous Organization of Single CdTe Nanoparticles into Luminescent Nanowires. *Science* **2002**, *297*, 237–240.
65. Querejeta-Fernandez, A.; Hernandez-Garrido, J. C.; Yang, H. X.; Zhou, Y. L.; Varela, A.; Parras, M.; Calvino-Gamez, J. J.; Gonzalez-Calbet, J. M.; Green, P. F.; Kotov, N. A. Unknown Aspects of Self-Assembly of PbS Microscale Superstructures. *ACS Nano* **2012**, *6*, 3800–3812.
66. NIST-XPS database, version 3.5. http://srdata.nist.gov/xps/ (accessed Nov 30, 2011).
67. Moulder, J. F.; Stickle, W. F.; Sobol, P. E.; Bomben, K. D. *Handbook of X-Ray Photoelectron Spectroscopy*; Perkin-Elmer: Eden Prairie, MN, 1992.
68. Singh, A.; Geaney, H.; Laffir, F.; Ryan, K. M. Colloidal Synthesis of Wurtzite Cu_2ZnSnS_4 Nanorods and Their Perpendicular Assembly. *J. Am. Chem. Soc.* **2012**, *134*, 2910–2913.
69. Gebauer, D.; Volkel, A.; Colfen, H. Stable Prenucleation Calcium Carbonate Clusters. *Science* **2008**, *322*, 1819–1822.
70. Lee, K.; Wagermaier, W.; Masic, A.; Kommareddy, K. P.; Bennet, M.; Manjubala, I.; Lee, S. W.; Park, S. B.; Colfen, H.; Fratzl, P. Self-assembly of Amorphous Calcium Carbonate Microlens Arrays. *Nat. Commun.* **2012**, *3*, 1–7.
71. Cong, H. P.; Ren, X. C.; Yao, H. B.; Wang, P.; Colfen, H.; Yu, S. H. Synthesis and Optical Properties of Mesoporous *b*-$Co(OH)_2$/Brilliant Blue G (G250) Hybrid Hierarchical Structures. *Adv. Mater.* **2012**, *24*, 1309–1315.
72. Critchley, K.; Khanal, B. P.; Gorzny, M. L.; Vigderman, L.; Evans, S. D.; Zubarev, E. R.; Kotov, N. A. Near-Bulk Conductivity of Gold Nanowires as Nanoscale Interconnects and the Role of Atomically Smooth Interface. *Adv. Mater.* **2010**, *22*, 2338–2342.
73. Leong, J. Y.; Yee, J. H. Hall-Effect in Reactively Sputtered Cu_2S. *Appl. Phys. Lett.* **1979**, *35*, 601–602.